

# Supporting Information

## Highly Monodisperse $\text{Cu}_3\text{Mo}_2\text{O}_9$ Micropompons with Excellent Performance in Photocatalysis, Photocurrent Response and Lithium Storage

Juan Xia,<sup>a</sup> Le Xin Song,<sup>\*a,b</sup> Wei Liu,<sup>\*a</sup> Yue Teng,<sup>a</sup> Qing Shan Wang,<sup>b</sup> Li Zhao<sup>b</sup> and Mao Mao Ruan<sup>b</sup>

<sup>a</sup> CAS Key Laboratory of Materials for Energy Conversion, Department of Materials Science and Engineering, University of Science and Technology of China, Jin Zhai Road 96, Hefei 230026, China

<sup>b</sup> Department of Chemistry, University of Science and Technology of China, Jin Zhai Road 96, Hefei 230026, China.

E-mail: solexin@ustc.edu.cn; wliu@ustc.edu.cn

### A list of the contents for all the supporting information

Pages	Contents
1	A table of contents page
2	<b>Figure S1.</b> The XRD patterns of $\text{NiMoO}_4 \cdot x\text{H}_2\text{O}$ (a), $\text{Cu}_3(\text{OH})_2(\text{MoO}_4)_2$ (b) and $\text{Zn}_3(\text{OH})_2(\text{MoO}_4)_2$ (c).
3	<b>Figure S2.</b> FE-SEM image of $\text{NiMoO}_4 \cdot x\text{H}_2\text{O}$ .
4	<b>Figure S3.</b> FE-SEM images of $\text{Cu}_3(\text{OH})_2(\text{MoO}_4)_2$ (a) and $\text{Zn}_3(\text{OH})_2(\text{MoO}_4)_2$ (b).
5	<b>Figure S4.</b> XRD pattern of $\text{ZnMoO}_4 \cdot 0.8\text{H}_2\text{O}$ .
6	<b>Figure S5.</b> XRD patterns of $\text{NiMoO}_4 \cdot x\text{H}_2\text{O}$ (a) and $\text{Cu}_3(\text{OH})_2(\text{MoO}_4)_2$ (c) obtained at 383 K for heating time of 10 h with a 2:1 initial molar ratio of Mo to Ni and Mo to Cu; $\alpha\text{-NiMoO}_4$ (b) and $\text{Cu}_3\text{Mo}_2\text{O}_9$ (d) were their sintering products at 873 K for 3 h.
7	<b>Figure S6.</b> FE-SEM image of $\text{ZnMoO}_4 \cdot 0.8\text{H}_2\text{O}$ .
8	<b>Figure S7.</b> The evolution of the precursor $\text{Cu}_3(\text{OH})_2(\text{MoO}_4)_2$ performed at 383 K for heating times of 0.5, 1, 3, 5 and 10 h.
9	<b>Figure S8.</b> XRD pattern of the $(\text{NH}_4)_2\text{Cu}(\text{MoO}_4)_2$ obtained by changing water to anhydrous ethanol at 383 K for heating time of 10 h. <b>Figure S9.</b> FE-SEM image of the $(\text{NH}_4)_2\text{Cu}(\text{MoO}_4)_2$ obtained by changing water to anhydrous ethanol at 383 K for heating time of 10 h.
10	<b>Figure S10.</b> XRD patterns of the $\text{Cu}_3(\text{OH})_2(\text{MoO}_4)_2$ materials obtained at 383 K for heating time of 0.5 h in the presence of HCl (a), HAc (b) and $\text{H}_4\text{Y}$ (c).
11	<b>Figure S11.</b> FE-SEM images of the $\text{Cu}_3(\text{OH})_2(\text{MoO}_4)_2$ materials obtained at 383 K for heating time of 10 h in the presence of HCl (a) and HAc (b).
12	<b>Figure S12.</b> XRD patterns of the $\text{Cu}_3(\text{OH})_2(\text{MoO}_4)_2$ microurchins (a) and $\text{Cu}_3\text{Mo}_2\text{O}_9$ micropompons (b).
13	<b>Figure S13.</b> XRD patterns of the spherical $\text{Cu}_3(\text{OH})_2(\text{MoO}_4)_2$ material prepared at 383 K for 10 h in the presence of 0.10 (a) and 0.30 g (b) $\text{H}_4\text{Y}$ . <b>Figure S14.</b> FE-SEM images of the spherical $\text{Cu}_3(\text{OH})_2(\text{MoO}_4)_2$ material prepared at 383 K for 10 h in the presence of 0.10 (a) and 0.30 g (b) $\text{H}_4\text{Y}$ .
14	<b>Figure S15.</b> FE-SEM images of the $(\text{NH}_4)_2\text{Cu}(\text{MoO}_4)_2$ materials obtained at 383 K for heating time of 0.5 h in the absence (a) and presence (b) of $\text{Na}_2\text{H}_2\text{Y}$ .
15	<b>Figure S16.</b> TG curve of the $\text{Cu}_3(\text{OH})_2(\text{MoO}_4)_2$ microurchins in air at a heating rate of $10.0 \text{ K min}^{-1}$ .
16	<b>Figure S17.</b> FTIR spectrum of the $\text{Cu}_3\text{Mo}_2\text{O}_9$ micropompons.
17	<b>Figure S18.</b> XRD patterns of the $\text{Cu}_3\text{Mo}_2\text{O}_9$ materials obtained by sintering the $\text{Cu}_3(\text{OH})_2(\text{MoO}_4)_2$ microurchins at 773 (a) and 973 K (b) for 3 h under air condition. <b>Figure S19.</b> FE-SEM images of the $\text{Cu}_3\text{Mo}_2\text{O}_9$ materials obtained by sintering the $\text{Cu}_3(\text{OH})_2(\text{MoO}_4)_2$ microurchins at 773 (a) and 973 K (b) for 3 h under air condition.
18	<b>Figure S20.</b> Field dependence of magnetization of the $\text{Cu}_3(\text{OH})_2(\text{MoO}_4)_2$ microurchins at 2 K in the applied fields: from $-50000$ to $50000$ Oe (a), temperature dependence of magnetization of the $\text{Cu}_3(\text{OH})_2(\text{MoO}_4)_2$ microurchins at 100 Oe from 2 to 300 K (b), a sketch map of linear extrapolation in achieving Curie temperature ( $T_C$ ) from 2 to 40 K (c), and an illustration of M/T differential coefficient method (d) in obtaining Curie temperature from 2 to 40 K.
19	<b>Figure S21.</b> $\text{N}_2$ adsorption-desorption isotherm and pore size distribution (inset) of the $\text{Cu}_3\text{Mo}_2\text{O}_9$ micropompons.
20	<b>Figure S22.</b> UV-Vis absorption spectra of the R6G solutions before and after being treated by the $\text{Cu}_3\text{Mo}_2\text{O}_9$ micropompons for 150 min.

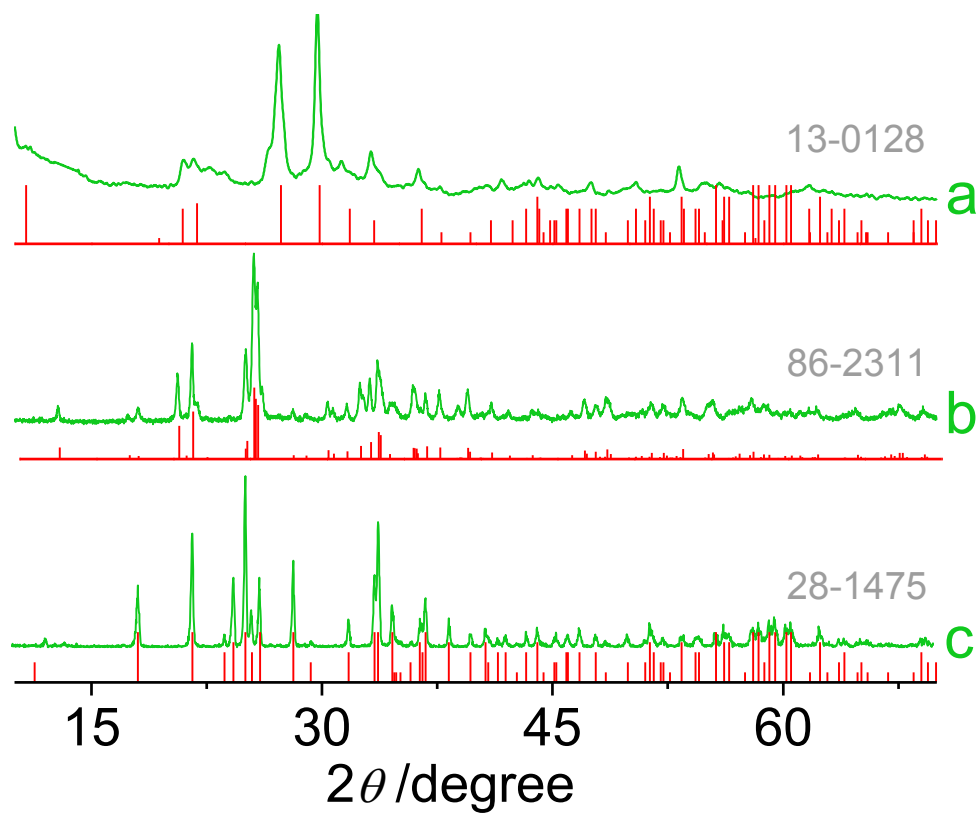


**Figure S1.** The XRD patterns of  $\text{NiMoO}_4 \cdot x\text{H}_2\text{O}$  (a),  $\text{Cu}_3(\text{OH})_2(\text{MoO}_4)_2$  (b) and  $\text{Zn}_3(\text{OH})_2(\text{MoO}_4)_2$  (c).

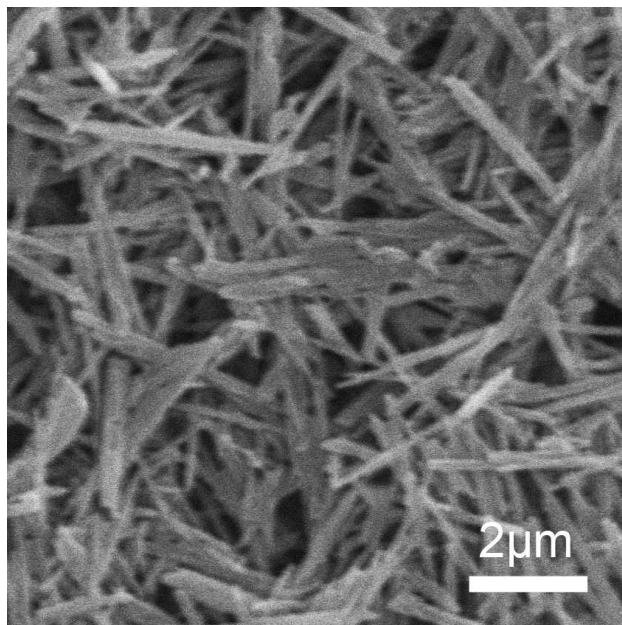


**Figure S2.** FE-SEM image of  $\text{NiMoO}_4 \cdot x\text{H}_2\text{O}$ .

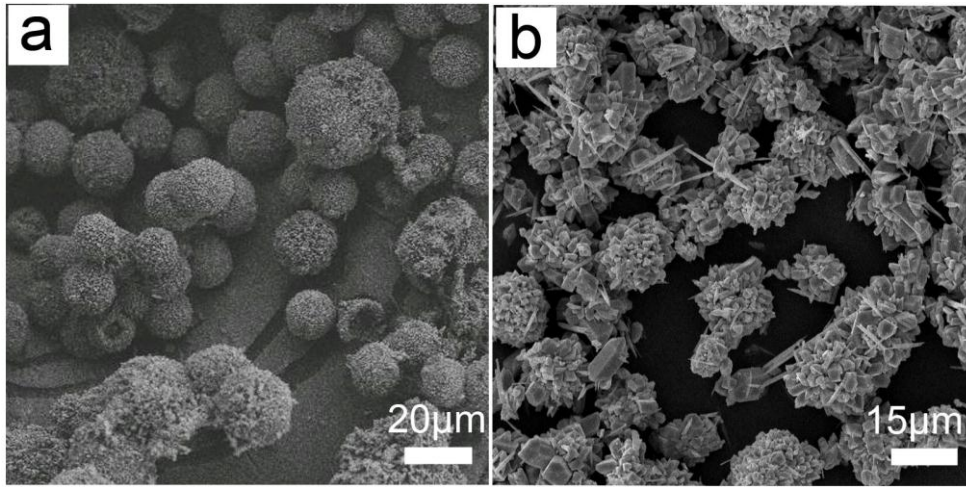


**Figure S3.** FE-SEM images of  $\text{Cu}_3(\text{OH})_2(\text{MoO}_4)_2$  (a) and  $\text{Zn}_3(\text{OH})_2(\text{MoO}_4)_2$  (b).

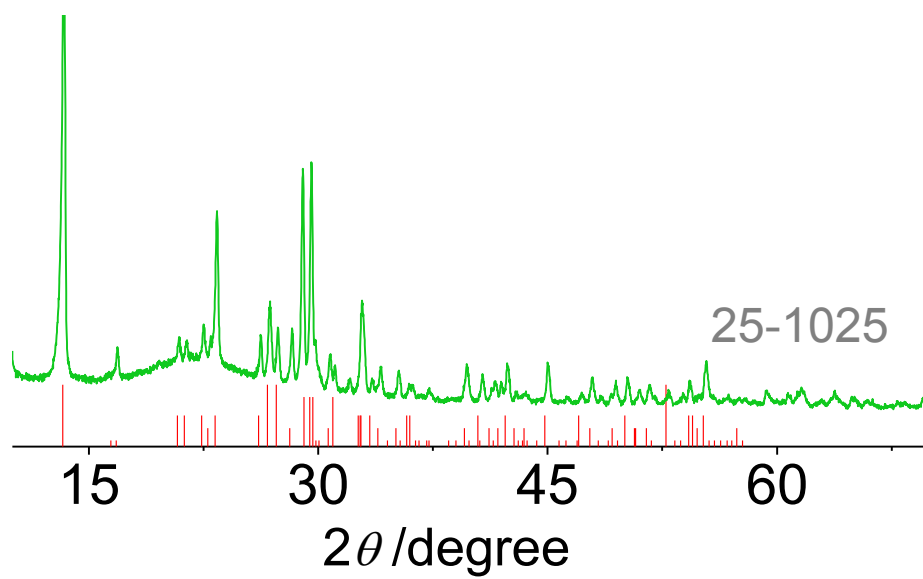


**Figure S4.** XRD pattern of  $\text{ZnMoO}_4 \cdot 0.8\text{H}_2\text{O}$ .

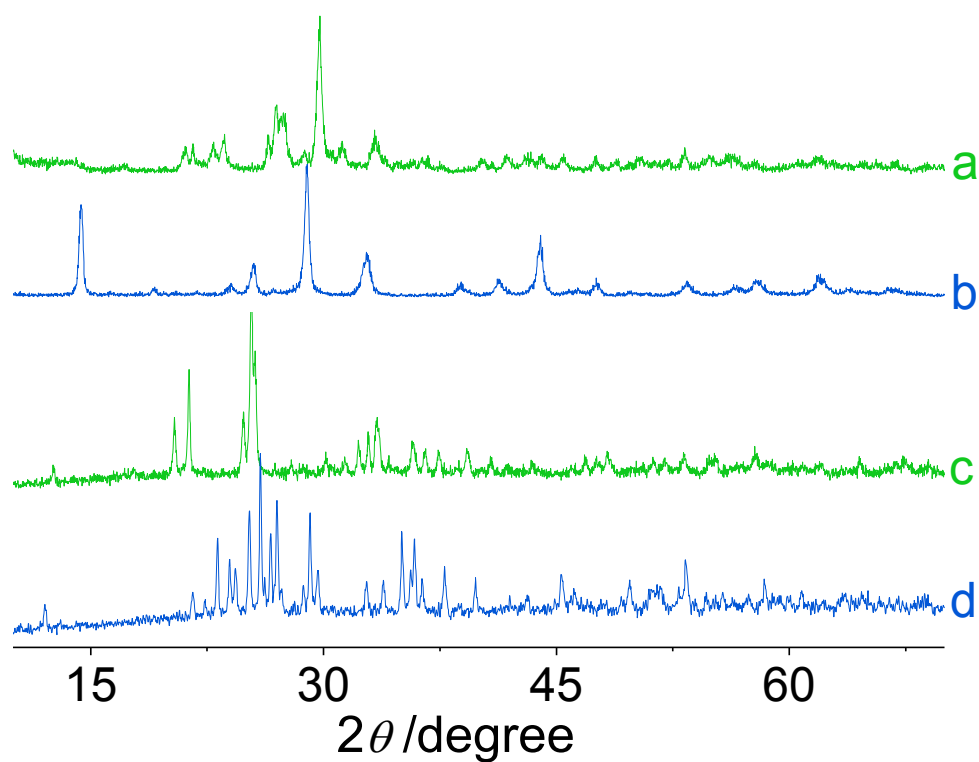


**Figure S5.** XRD patterns of  $\text{NiMoO}_4 \cdot x\text{H}_2\text{O}$  (a) and  $\text{Cu}_3(\text{OH})_2(\text{MoO}_4)_2$  (c) obtained at 383 K for heating time of 10 h with a 2:1 initial molar ratio of Mo to Ni and Mo to Cu;  $\alpha\text{-NiMoO}_4$  (b) and  $\text{Cu}_3\text{Mo}_2\text{O}_9$  (d) were their sintering products at 873 K for 3 h.

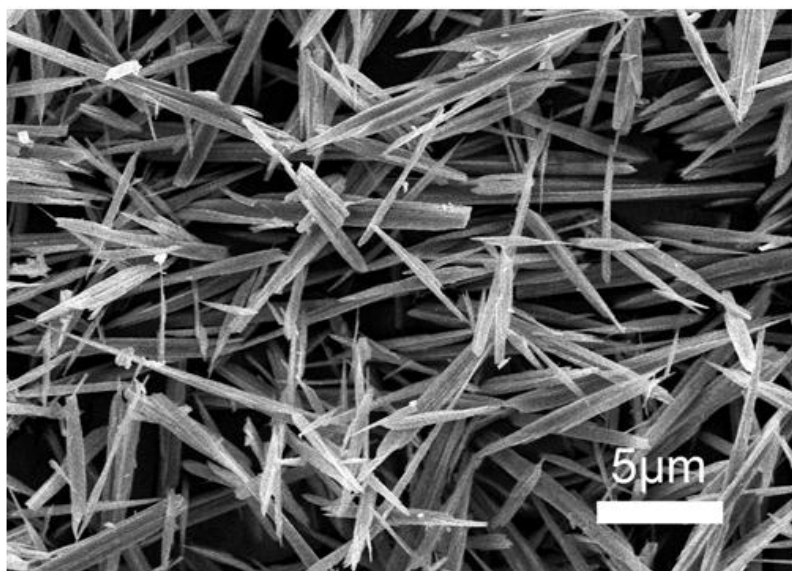


**Figure S6.** FE-SEM image of ZnMoO<sub>4</sub> · 0.8H<sub>2</sub>O.

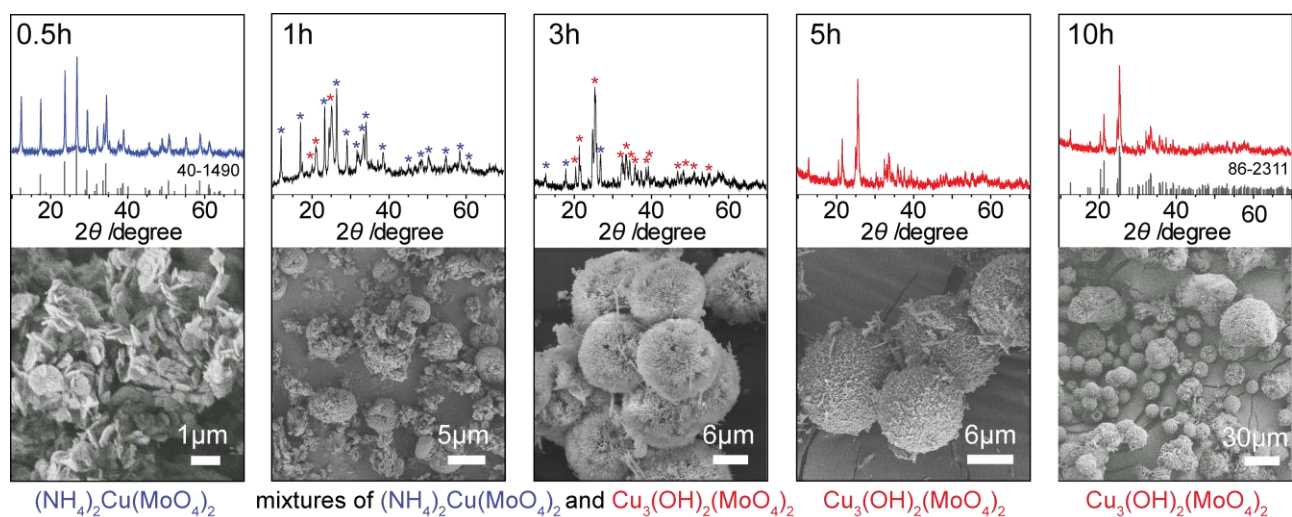


**Figure S7.** The evolution of the precursor  $\text{Cu}_3(\text{OH})_2(\text{MoO}_4)_2$  performed at 383 K for heating times of 0.5, 1, 3, 5 and 10 h.



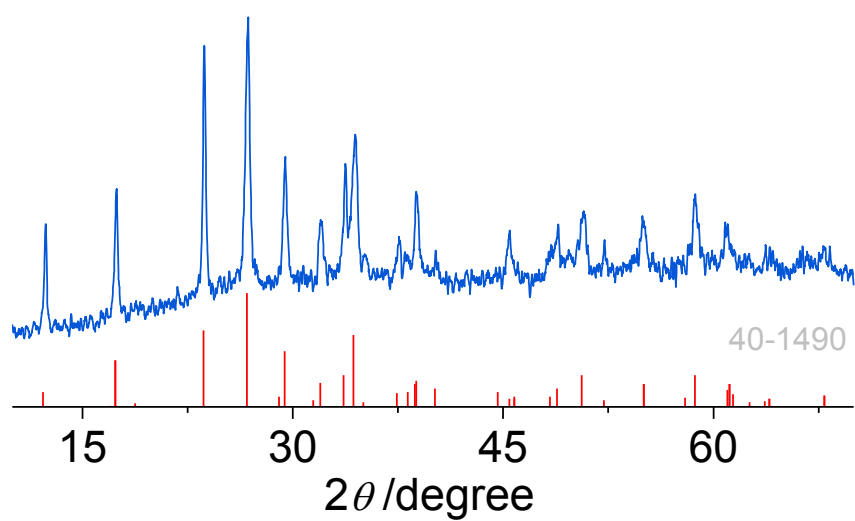


**Figure S8.** XRD pattern of the  $(\text{NH}_4)_2\text{Cu}(\text{MoO}_4)_2$  obtained by changing water to anhydrous ethanol at 383 K for heating time of 10 h.

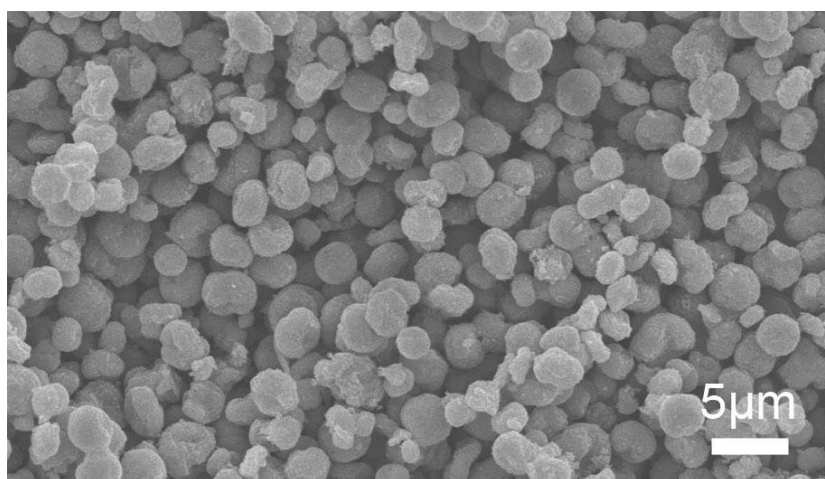


**Figure S9.** FE-SEM image of the  $(\text{NH}_4)_2\text{Cu}(\text{MoO}_4)_2$  obtained by changing water to anhydrous ethanol at 383 K for heating time of 10 h.

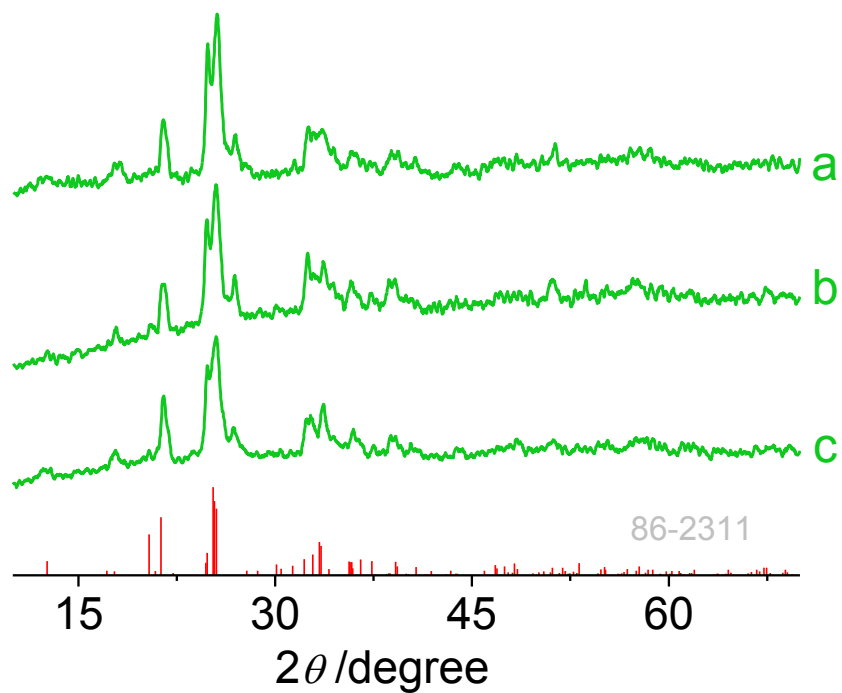


**Figure S10.** XRD patterns of the  $\text{Cu}_3(\text{OH})_2(\text{MoO}_4)_2$  materials obtained at 383 K for heating time of 0.5 h in the presence of HCl (a), HAc (b) and  $\text{H}_4\text{Y}$  (c).

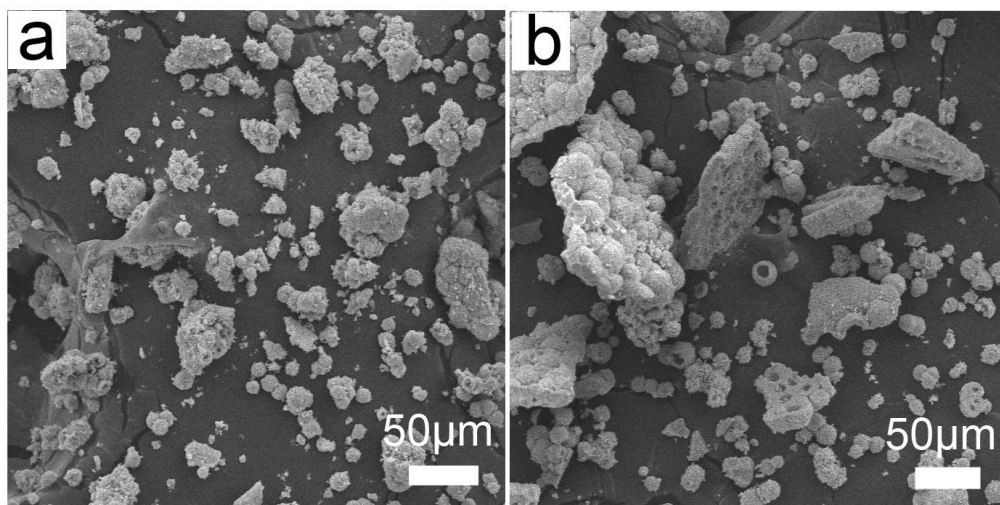


**Figure S11.** FE-SEM images of the  $\text{Cu}_3(\text{OH})_2(\text{MoO}_4)_2$  materials obtained at 383 K for heating time of 10 h in the presence of HCl (a) and HAc (b).

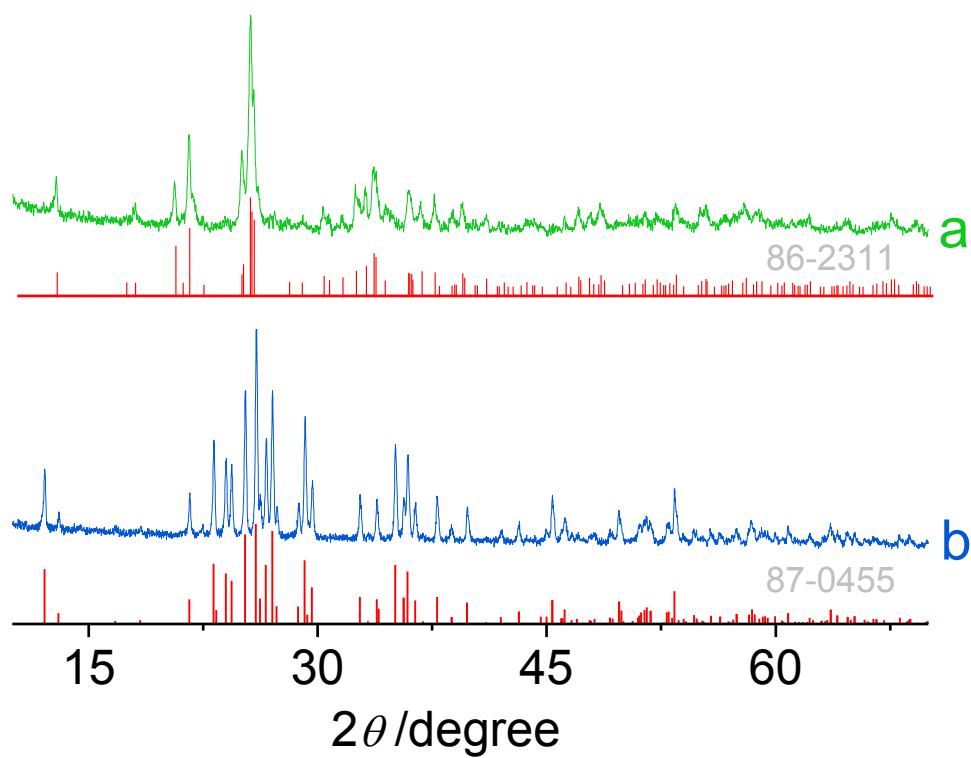


**Figure S12.** XRD patterns of the  $\text{Cu}_3(\text{OH})_2(\text{MoO}_4)_2$  microrurchins (a) and  $\text{Cu}_3\text{Mo}_2\text{O}_9$  micropompons (b).

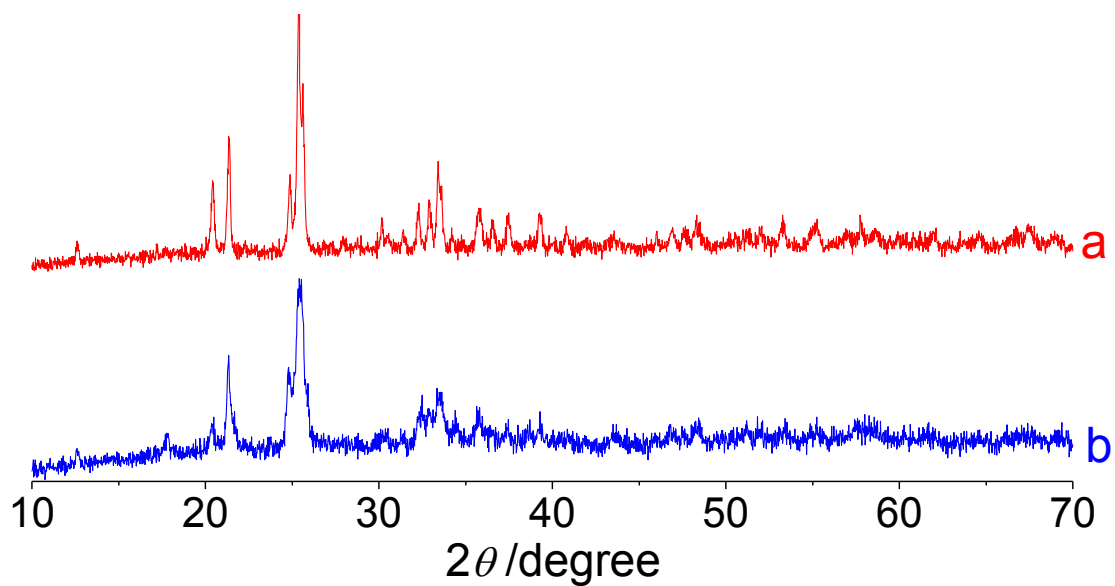


**Figure S13.** XRD patterns of the spherical  $Cu_3(OH)_2(MoO_4)_2$  material prepared at 383 K for 10 h in the presence of 0.10 (a) and 0.30 g (b)  $H_4Y$ .

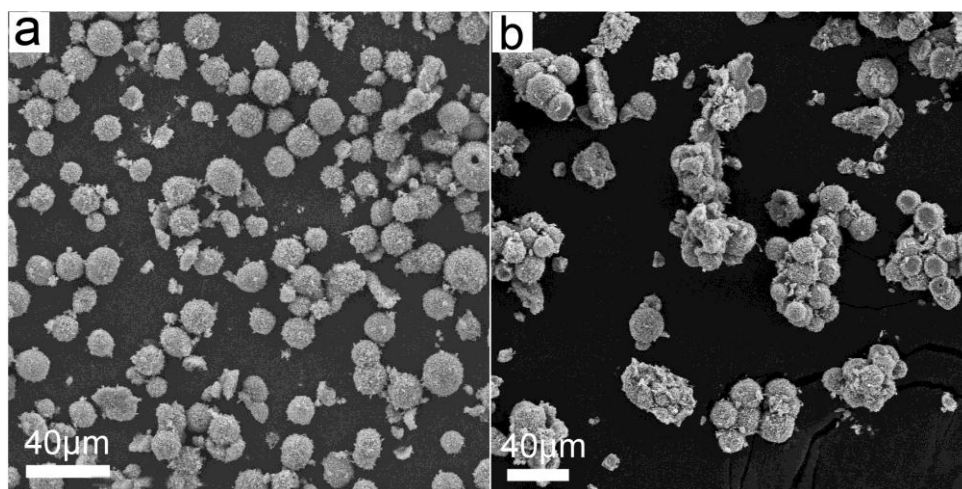


**Figure S14.** FE-SEM images of the spherical  $Cu_3(OH)_2(MoO_4)_2$  material prepared at 383 K for 10 h in the presence of 0.10 (a) and 0.30 g (b)  $H_4Y$ .

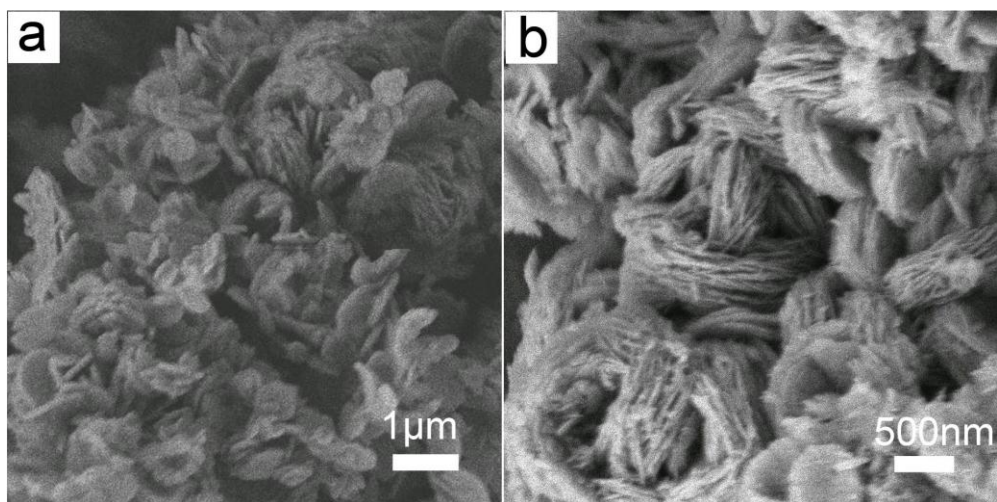


**Figure S15.** FE-SEM images of the  $(\text{NH}_4)_2\text{Cu}(\text{MoO}_4)_2$  materials obtained at 383 K for heating time of 0.5 h in the absence (a) and presence (b) of  $\text{Na}_2\text{H}_2\text{Y}$ .

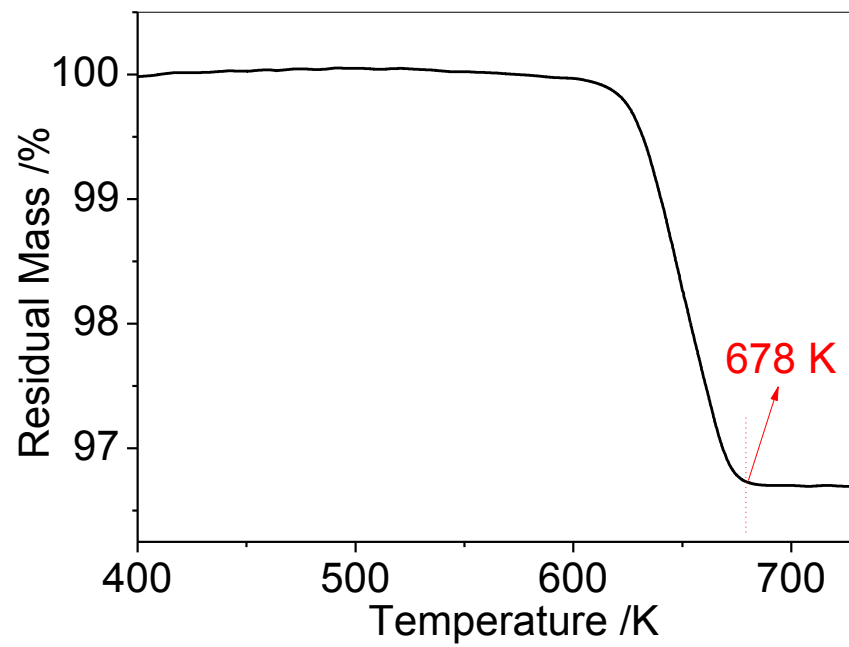


**Figure S16.** TG curve of the  $\text{Cu}_3(\text{OH})_2(\text{MoO}_4)_2$  microurchins in air at a heating rate of  $10.0 \text{ K min}^{-1}$ .

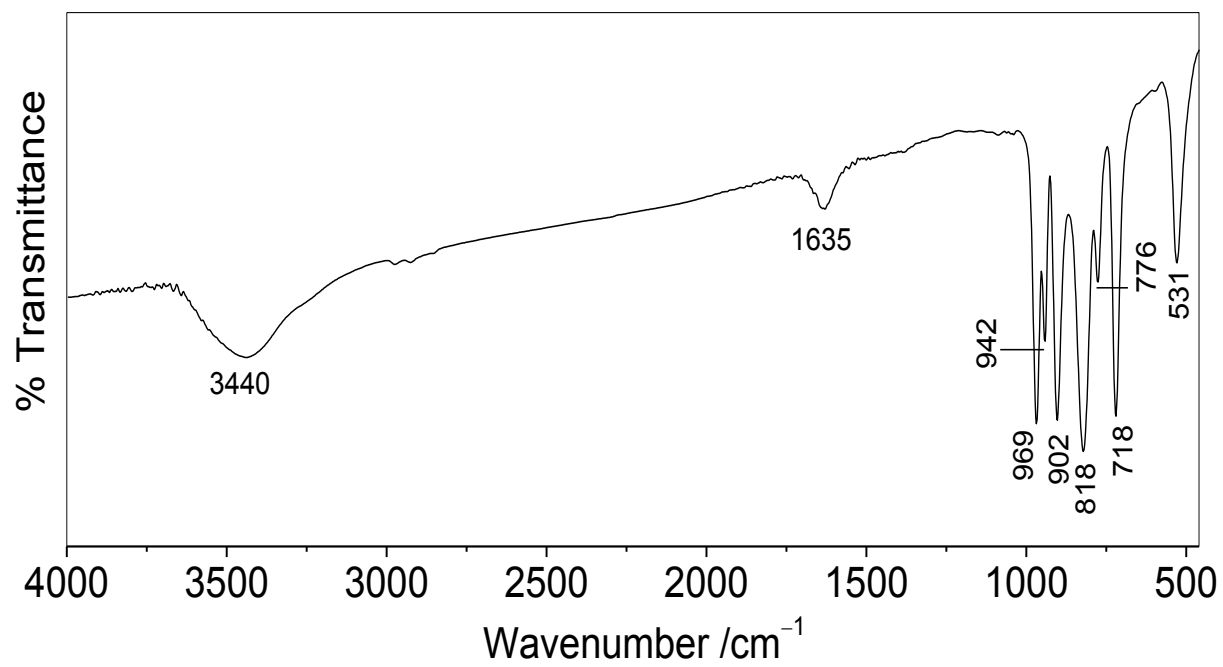


**Figure S17.** FTIR spectrum of the Cu<sub>3</sub>Mo<sub>2</sub>O<sub>9</sub> micropompons.



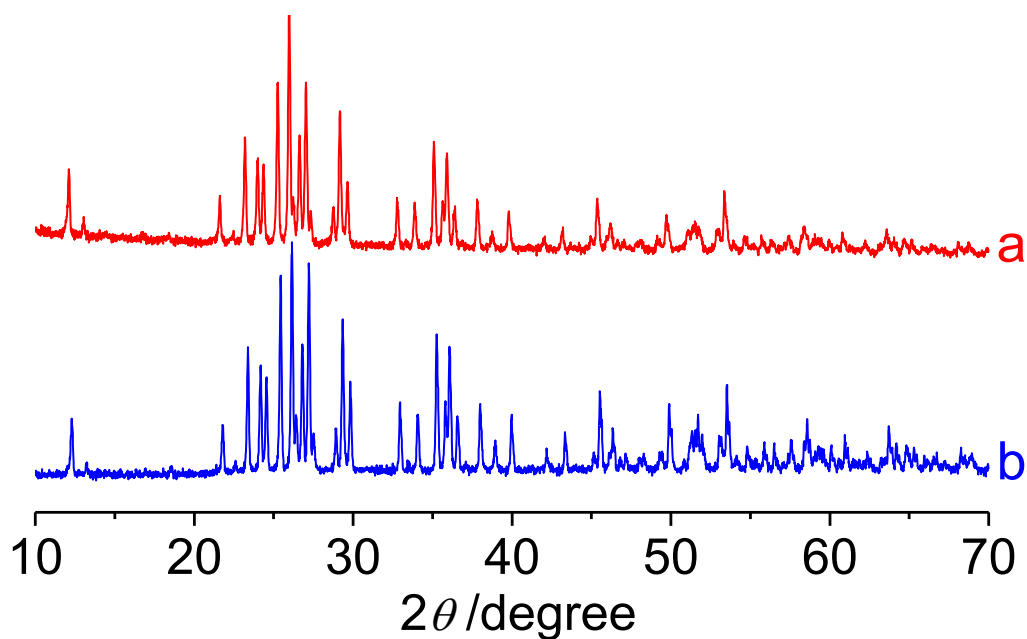


**Figure S18.** XRD patterns of the  $\text{Cu}_3\text{Mo}_2\text{O}_9$  materials obtained by sintering the  $\text{Cu}_3(\text{OH})_2(\text{MoO}_4)_2$  microrouchins at 773 (a) and 973 K (b) for 3 h under air condition.

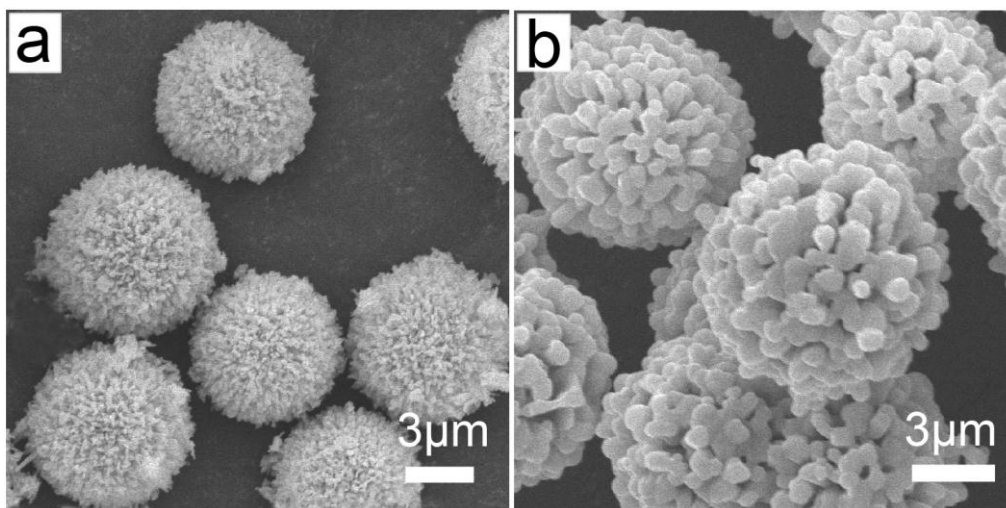


**Figure S19.** FE-SEM images of the  $\text{Cu}_3\text{Mo}_2\text{O}_9$  materials obtained by sintering the  $\text{Cu}_3(\text{OH})_2(\text{MoO}_4)_2$  microrouchins at 773 (a) and 973 K (b) for 3 h under air condition.

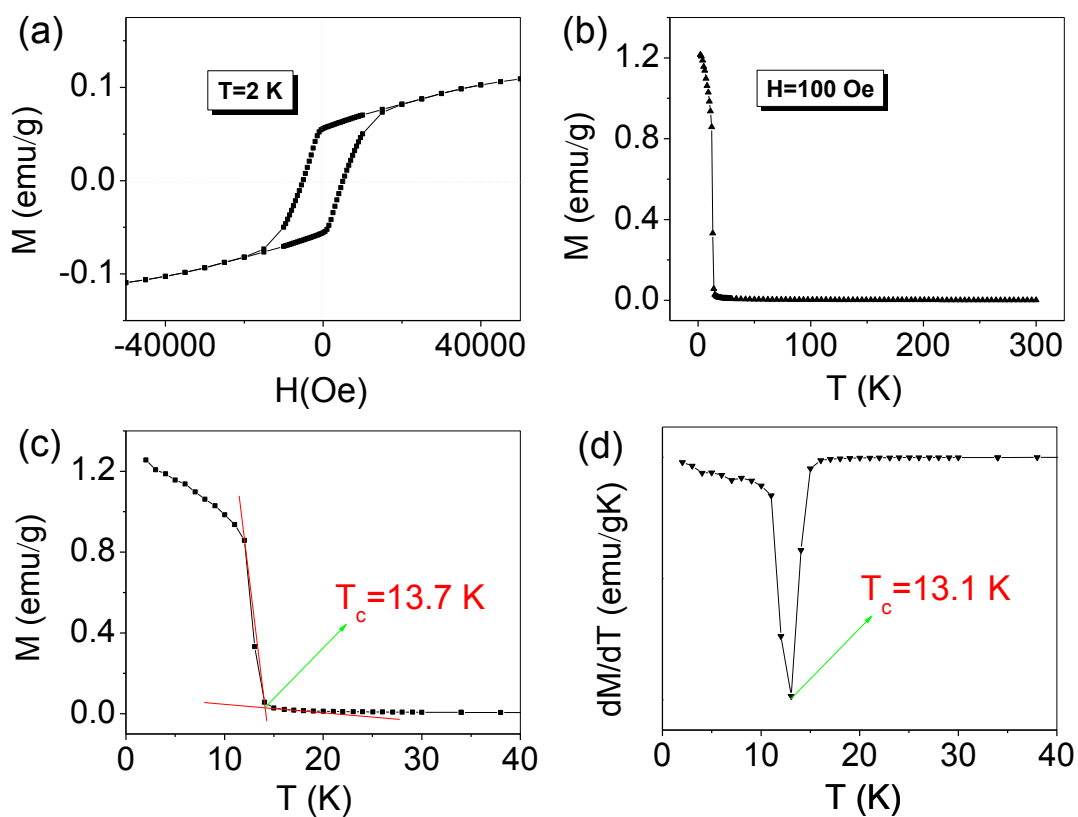


**Figure S20.** Field dependence of magnetization of the  $\text{Cu}_3(\text{OH})_2(\text{MoO}_4)_2$  microrouchins at 2 K in the applied fields: from  $-50000$  to  $50000$  Oe (a), temperature dependence of magnetization of the  $\text{Cu}_3(\text{OH})_2(\text{MoO}_4)_2$  microrouchins at 100 Oe from 2 to 300 K (b), a sketch map of linear extrapolation in achieving Curie temperature ( $T_c$ ) from 2 to 40 K (c), and an illustration of  $M/T$  differential coefficient method (d) in obtaining  $T_c$  from 2 to 40 K.

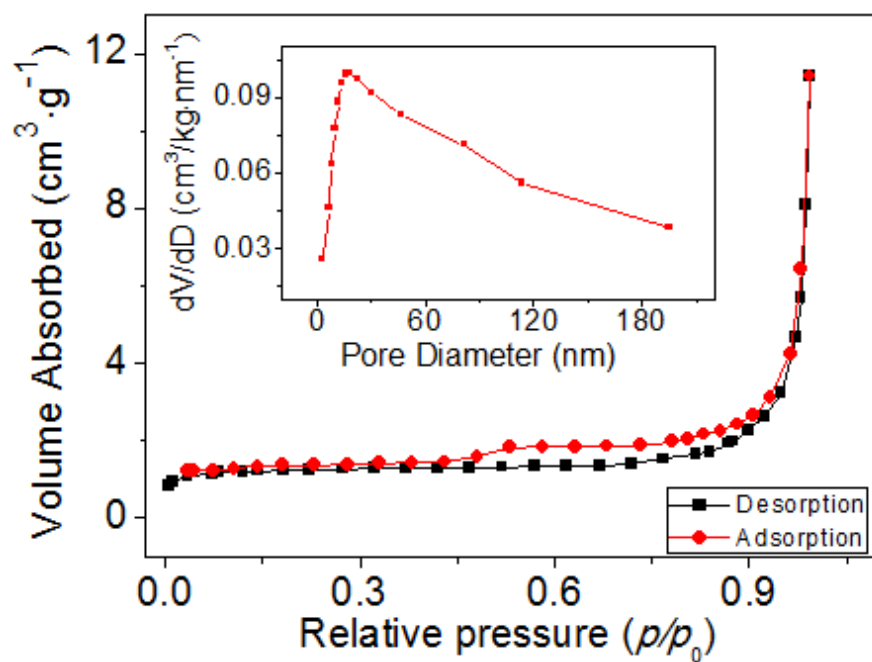


**Figure S21.**  $\text{N}_2$  adsorption-desorption isotherm and pore size distribution (inset) of the  $\text{Cu}_3\text{Mo}_2\text{O}_9$  micropompons.

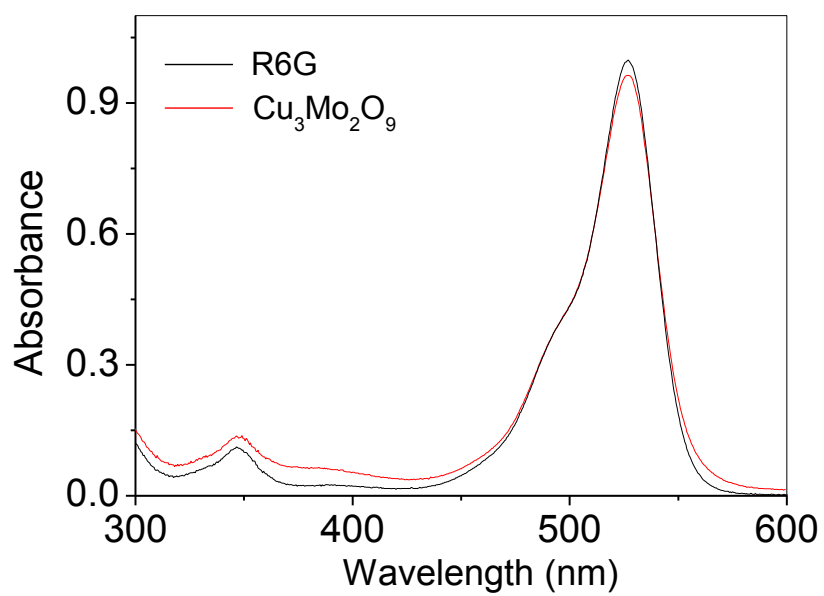


**Figure S22.** UV-Vis absorption spectra of the R6G solutions before and after being treated by the  $\text{Cu}_3\text{Mo}_2\text{O}_9$  micropompons for 150 min.